Improving and Extending the Phases of Medium- and Low-Resolution Macromolecular Structure Factors by Density Modification

By Richard W. Schevitz, Alberto D. Podjarny,* Martin Zwick,† John J. Hughes‡ and Paul B. Sigler

Department of Biophysics and Theoretical Biology, The University of Chicago, 920 East 58th Street, Chicago, Illinios 60637, USA

Abstract

Non-negativity of the electron density function and constancy of the solvent regions were exploited to improve 2633 phases of crystalline yeast $tRNA_f^{Met}$ ($P6_422$, $a = 115\cdot3$, $c = 137\cdot9$ Å, $z = 12$), which had been obtained by multiple isomorphous replacement (MIR) in the resolution zone 14–4·5 Å. Phases were also determined for an additional 912 reflections not previously phased by MIR from the resolution range 100 to 4 Å, the very limits of the diffraction pattern. An iterative procedure was employed in which phases for each cycle were calculated from a density map modified by imposing the above constraints and were combined with the observed amplitudes to produce a new and improved map. Initially phases calculated in each cycle were merged with the original MIR phase probability curve; convergence was achieved in seven cycles. The phases were then released from the MIR analysis by using just the calculated phases until a second convergence was achieved (four cycles). The average difference between the experimental phases and phases calculated from the refined coordinates was reduced from 68° for the original MIR analysis to 43° by the use of these real-space direct methods. Phases determined solely by density modification were as accurate as the original MIR phase set. The map calculated with improved and extended phases was dramatically superior to the MIR map and even approached in quality the map produced with phases calculated from the refined molecular coordinates.

Introduction

Density modification is a method for improving and/or extending a set of phases by applying prior knowledge about the electron density distribution. This is done by imposing known constraints in real space directly on the density function through appropriate modifications of the map. New and presumably improved phases are calculated from the modified map and these can simply be combined with observed amplitudes to produce the density map for the next cycle. (Often, the initial phases, the phases of the previous cycle, and/or the amplitudes calculated from the modified map are also used in generating the new map.) The procedure is iterated until some criterion of convergence is met. The advantage of this approach over purely reciprocal-space direct methods is the ease and straightforwardness of imposing real-space constraints and the availability of the fast Fourier transform (FFT) to reduce computational requirements.

The method is highly flexible, allowing the investigator to exploit whatever constraint exists in the structure under study. At very high resolution, the atomicity of the density function can be used, in a manner very similar, if not formally equivalent, to the way this constraint is used in many reciprocal-space methods. In certain structures the constraint might be the high degree of noncrystallographic symmetry and/or the uniform character of the solvent. The electron density of all molecular structures must be greater than zero and less than generally known maxima, and all maps of proteins and nucleic acids should have continuous density for the polymeric backbone. The investigator is also free to intervene, where appropriate, to weight up or down the relative influence of any particular constraint and to introduce phase information from external sources. Most importantly, the procedure can be sensibly applied at any resolution. The convenience afforded by the real-space modification steps is enhanced by the reciprocal-space step which alternates with it, *i.e.* there are many ways that amplitudes and phases can be chosen to generate the next density map and this contributes significantly to the flexibility of the approach.

Density modification techniques were first applied under the name of 'phase correction' to crystals of small molecules at high resolution (Hoppe & Gassmann, 1968). The application to macromolecules has

© 1981 International Union of Crystallography

been pursued by several investigators since it offers the possibility of improving an electron density map determined by multiple isomorphous replacement (MIR) or by molecular replacement without additional information or any provisional molecular interpretation of the map. Barrett & Zwick (1971), introducing the fast Fourier algorithm to facilitate computation, showed that the method could extend the resolution of the map of sperm-whale metmyoglobin from 3 to 2 Å resolution. Connectivity required by the molecular structure but not apparent in the 3 Å MIR map was present in the 2 Å extended map. The interpretability of the low-resolution electron density maps of myohemerythrin (Hendrickson, Klippenstein & Ward, 1975) and hemerythrin (Ward, Hendrickson & Klippenstein, 1975) was enhanced by leveling the solvent regions of the cells containing these molecules. Starting with a 2·0 Å MIR map of rubredoxin, Collins and co-workers (Collins, Cotton, Hazen, Meyer & Morimoto, 1975; Collins, Brice, La Cour & Legg, 1976) reduced the mean discrepancy between the experimental phases and those calculated from the refined model coordinates from 44 to 37°. Concomitantly, they extended the phases to 1·5 Å with a phase error* of 41°. This was achieved by truncating the negative density and replacing the positive density ρ with $3\rho^2 - 2\rho^3$. To date the most dramatic application of density modification has been the successful exploitation of the high degree of noncrystallographic symmetry found in crystals of viruses (Harrison, Olson, Schutt, Winkler & Bricogne, 1978; Abad-Zapatero et al., 1980) and their subunits (Bloomer, Champness, Bricogne, Staden & Klug, 1978), as well as certain oligomeric enzymes (Argos, Ford & Rossmann, 1975; Biesecker, Harris, Thierry, Walker & Wonacott, 1977). In another use of redundant information, Fletterick & Steitz (1976) have combined phase information from separate structure determinations of the same enzyme in different crystal forms to improve their electron density map.

We have employed a simple yet powerful technique of density modification that uses both solvent leveling and attenuation of negative density. It is an iterative procedure that tends to hold apparently reliable phases close to their starting values in the early cycles to aid convergence (Bricogne, 1976). This paper also describes the dramatic improvement and extension of phases when applied to yeast tRNA$_f^{\text{Met}}$ at 4·0 Å resolution.

The characteristics of this crystal are summarized in Table 1. The lattice is poorly ordered, exhibiting no measurable intensities beyond 4·0 Å. Although there is no local symmetry to exploit, solvent occupies 82·5%

---

* Throughout this paper the term 'error' when applied to phases refers to the discrepancy between the phases under consideration and the phase calculated from the atomic coordinates of the refined structure.

of the crystal's volume, making this crystal structure particularly amenable to density modification by solvent leveling.

Table 1. *Characteristics of yeast tRNA$_f^{\text{Met}}$ crystals*

Space group $P6_4 22$
12 general positions
1 molecule per asymmetric unit
$a = 115\cdot3, c = 136\cdot9$ Å
$B \simeq 150$
Solvent: 2·6 M $(NH_4)_2SO_4$.
      5 mM Mg^{2+} 2 mM spermine
      5 mM cacodylate, pH 5·0
Solvent volume fraction: 82·5%

Methods

The starting MIR phase set

MIR phases for yeast tRNA$_f^{\text{Met}}$ were derived from heavy-atom derivatives solved with difference maps using phases calculated from refined native tRNA$_f^{\text{Met}}$ coordinates (Podjarny, Schevitz, Sussman & Sigler, 1980). The latter were determined from a 4 Å refinement based on the 6 Å structure previously reported by Schevitz, Podjarny, Krishnamachari, Hughes & Sigler (1979). This model had a conventional R value of 0·25 to 4 Å resolution after a least-squares procedure that linked together constrained ribose, phosphate and base groups by distance restraints (Sussman, Holbrook, Church & Kim, 1977). The phases, calculated from the refined tRNA coordinates, were used *only* to find the heavy-atom positions and later to provide a reference for monitoring the quality of the phases produced by the procedures described below. In all other respects
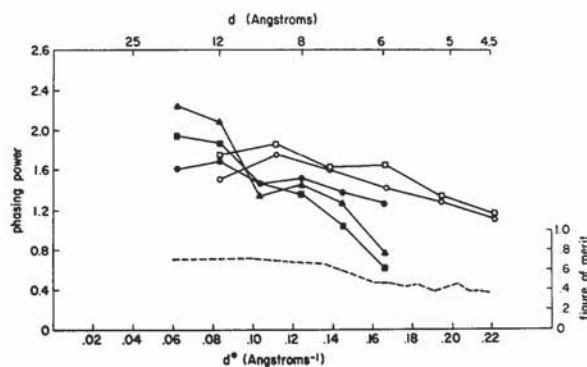

Fig. 1. Phasing power $[\sum_h |F_H|^2]^{1/2}/[\sum_h (|F_{PH}^o| - |F_{PH}^c|)^2]^{1/2}$ of five isomorphous derivatives used in the MIR analysis of yeast tRNA$_f^{\text{Met}}$ plotted against resolution. They are gadolinium, lightly substituted, precession data (■); gadolinium, heavily substituted, precession data (▲); pyridyl mercury acetate, precession data (●); gadolinium, oscillation data (□), and pyridyl mercury acetate, oscillation data (○). Figure of merit (---) is determined from MIR phasing and has a mean value of 0·52 over 2633 reflections from 14 to 4·5 Å resolution. $|F_H|$ is the calculated heavy-atom structure amplitude; $(|F_{PH}^o| - |F_{PH}^c|)$ is the 'lack of closure' error between observed and calculated isomorphous derivative structure amplitudes for some reflection h.

the MIR phase analysis represents a genuine experimental situation and contains the usual errors and limitations that one normally encounters in a MIR analysis (Fig. 1). This was considered a more representative starting point than the original MIR phase set used to solve the structure (Schevitz *et al.*, 1979) as the latter phases contained a systematic error due to a consistent misassignment of the *z* coordinates of the heavy atoms.

6·0 Å precession data (parent and three derivatives) and 4·5 Å oscillation data (parent with two derivatives)
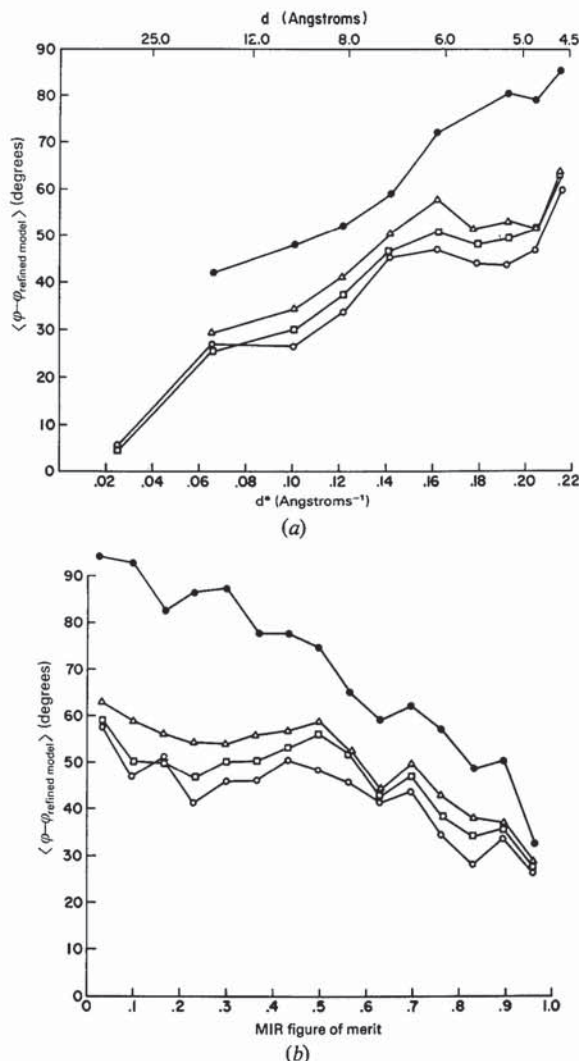

(a)

(b)

Fig. 2. Mean phase error following density modification with 4·5 Å yeast $tRNA_f^{Met}$ data *vs* (*a*) resolution and (*b*) the figure of merit of the starting phases determined by MIR. Plotted are the mean errors for (i) the starting 2633 MIR phases in the range 14–4·5 Å (●) having 68° average phase error, (ii) these 2633 MIR phases after tethered refinement (△) having 49° average phase error, (iii) the MIR phases after tethered refinement with extension (29 reflections added) to 100 Å resolution (□) having 46° average phase error and (iv) these 2662 MIR phases after tethered refinement with extension to 100 Å followed by untethered refinement (○) giving 43° average phase error.

were phased separately to minimize systematic errors and the phases merged by multiplying together their phase probability curves. The resultant curves were preserved for combination with density modification phase information by simply saving the four coefficients of the phase probability curves as formulated by Hendrickson & Lattman (1970).

$$P(\varphi) \propto \exp\left(A\cos\varphi + B\sin\varphi + C\cos 2\varphi + D\sin 2\varphi\right),$$

(1)

where P is the unnormalized probability of the phase φ being correct.

The MIR phases were compared with the phases calculated from the refined model (Podjarny *et al.*, 1980) and the error plotted separately as a function of both resolution (Fig. 2*a*) and MIR figure of merit (Fig. 2*b*). A mean error of 68° in the phase set reflects a suitably challenging experimental test case for phase improvement by density modification.

The density modification procedure

Fig. 3 summarizes the procedure used in this study. The first step was to calculate the starting 4·5 Å MIR electron density map of yeast $tRNA_f^{Met}$ using observed amplitudes $|F^o|$, centroid phases (φ^{MIR}) and figure of merit (m^{MIR}) (Blow & Crick, 1959). A $64 \times 64 \times 72$ grid was used for this cell, giving a grid spacing of 1·8 and 1·9 Å in the *a* and *c* directions respectively. The MIR electron density map is given in Fig. 4(*a*). The molecule was 'carved' out of the surrounding density by sectioning the map on transparent plastic sheets of scaled thickness and drawing a molecular boundary on each section (Fig. 4*b*). The boundary line was drawn in a smooth and conservative way that maintained continuity from section to section and did not follow detailed involutions or cut across substantial density. The molecular envelope contained 36% of the cell volume compared with a molecular volume fraction of 17·5% determined by crystal density flotation
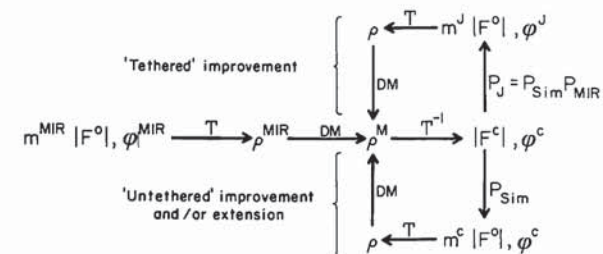

Fig. 3. Scheme used to improve and/or extend the MIR phases of yeast $tRNA_f^{Met}$. *T* refers to Fourier transformation. *DM* refers to density modification and φ^c the phase calculated from the modified map. P_{Sim} is the Sim probability curve described in the text which is unimodal and centered on φ^c and has an associated figure of merit m^c. P_J is the joint phase probability obtained by multiplying the MIR phase probability curve by P_{Sim}. φ^J is the centroid phase and m^J the figure of merit of P_J.
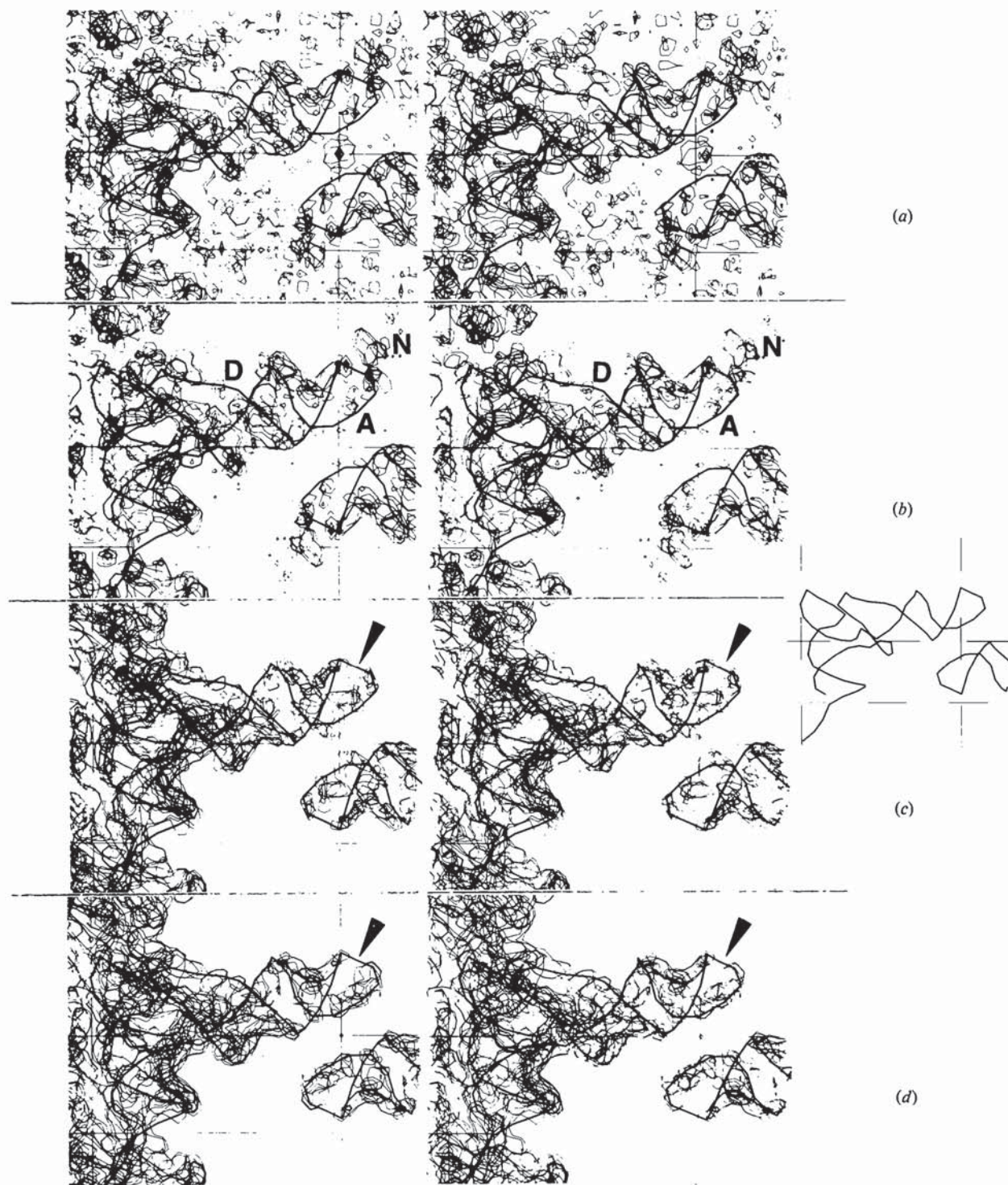
Fig. 4. Superposition of the refined phosphate backbone of yeast tRNA$_f^{Met}$ (see insert) on the electron density map calculated with the following coefficients: (a) $m^{MIR}\ |F^o|\ \exp\ i\varphi^{MIR}$ with 2633 terms from 14 to 4·5 Å resolution with mean figure of merit $\bar{m} = 0·51$, averaged discrepancy with phases calculated from refined coordinates $\bar{\varepsilon} = 68°$, and relative contour level $l = 0·46$; (b) 'carved' map produced by the same MIR phases as in (a) modified by solvent leveling and attenuation of negative density. Labeled are the anticodon loop (A), the D stem (D), and noise near the anticodon loop (N); (c) $m^c\ |F^o|\ \exp\ i\varphi^c$ following refinement and extension from 100 to 4·0 Å resolution by seven cycles of tethered and four cycles of untethered density modification with 3545 terms, $\bar{m} = 0·7$, $\bar{\varepsilon} = 49°$, and $l = 1·0$; the arrows point to the gap in the electron density at $P(33)$; (d) $|F^o|\ \exp\ i\varphi^R$ where φ^R are the phases calculated from refined coordinates using 3545 terms from 100 to 4 Å resolution, unit weights, and $l = 1·0$.

(Johnson, Adolph, Rosa, Hall & Sigler, 1970). This generous 'carving' procedure reflects our uncertainty of the exact boundaries of the molecule. Note the noise which was included in the carved map (Fig. 4b).

The density was modified in two ways: (a) the solvent region outside the molecular boundary was 'leveled' such that

$$\rho^{mod} = \rho \text{ for } \rho \text{ inside molecular boundary,}$$

$$\rho^{mod} = \langle \rho \rangle \text{ for } \rho \text{ outside the molecular boundary,}$$

where $\langle \rho \rangle$ is the average over all points which lie in the solvent; (b) the positivity of electron density was asserted by attenuating negative regions

$$\rho^{mod} = \rho \text{ for } \rho \geq 0$$

$$\rho^{mod} = 0 \cdot 1 \, \rho \text{ for } \rho < 0.$$

The $F(000)$ term was selected so that the average solvent level was approximately zero; this effectively began the attenuation of negative density at the average solvent level. Solvent leveling and attenuation of negative density were performed both separately and together to assess their individual and cooperative phasing powers.

The modified map was transformed by the fast Fourier algorithm *CHAFF* (Bantz & Zwick, 1974) yielding calculated amplitudes $|F^c|$ and phases φ^c. $|F^c|$ was compared with $|F^o|$ to estimate the reliability of φ^c by using Bricogne's (1976) adaptation of Sim's (1959) formula which gives the probability for any phase of a partially defined structure being correct as

$$P(\varphi) \propto \exp\left[2|F^o|\,|F^c|\cos(\varphi - \varphi^c)/\langle|F^o|^2 - |F^c|^2\rangle\right] \tag{2}$$

where $\langle|F^o|^2 - |F^c|^2\rangle$ is the mean difference between the observed and calculated intensities in a zone of resolution. From this formulation we obtain a figure of merit m^c for the phase φ^c. The modified Sim probability curve also permits us to merge the phase information obtained from density modification with that originally obtained from MIR by multiplying the two phase probability curves together. From this joint phase probability curve, we obtain a centroid phase φ^J and a corresponding figure of merit m^J.

The next cycle was initiated by calculating a new map with either of two alternative coefficients, $m^J|F^o| \exp(i\varphi^J)$ or $m^c|F^o|\exp(i\varphi^c)$. The new electron density map was modified and transformed to give a new set of $|F^c|$ and φ^c and the cycle was then repeated. Convergence was monitored by comparing the current values of $|F^c|$ and φ^c with both the original amplitude and phase values and the corresponding values from the last cycle (Fig. 5).

All calculations were performed using the program *DENMOD*, an extension of which has also been applied to phase refinement investigations of a small molecule by Zwick, Bantz & Hughes (1976). This program has the capability of utilizing an explicit phase or the A,B,C,D coefficients of the phase probability curves. Phase probability curves were multiplied together by simply adding these exponential coefficients. Molecular boundaries were read in as closed polygons defining molecular domains on a given plane. Core requirements for a $64 \times 64 \times 72$ grid are 490K bytes, and execution time for 11 cycles is 11 min. on an IBM 370/195.

Results

'Tethered' phase improvement in the resolution range 14–4·5 Å

Seven cycles of density modification combining solvent leveling and attenuation of negative density were applied to the electron-density map of yeast $t\text{RNA}_f^{Met}$. In this procedure we used the 2633 structure factors which were in the resolution range 14–4·5 Å and had been initially phased by MIR. In each cycle the phase probability distribution produced by density modification was merged with the initial MIR phase probability curve, a procedure hereafter called 'tethering.' Despite this close tethering of the phases in each cycle to the initial MIR phases, the final centroid phases of the joint curves changed from the initial MIR phases by a mean amount of 42°. Fig. 6 shows that the greatest phase change occurred in structure factors with the poorest initial MIR figure of merit. Thus those MIR phases judged to be least reliable were changed the most.

The final phases produced by density modification tethered to the original MIR phases had an average error of 49° compared to 68° for the original MIR phases. Thus the mean phase error was reduced by 19°. Fig. 2(a) shows that the improvement was significant at all levels of resolution, perhaps slightly better at higher resolution. Like the phase change, the phase improvement tended to be greatest for terms with the poorest original MIR figure of merit (Fig. 2b).

Phase extension to lower resolution in conjunction with tethered phase improvement

The procedure outlined above was repeated with 29 low-resolution (100–14 Å) amplitudes added to the data set, the majority of which were very intense and for a variety of technical reasons had not been phased by MIR. For the initial map these 29 structure factors were included with an initial weighted amplitude of 0·0 and an arbitrary phase of 0°. Had the map not been modified, the reverse Fourier transformation would have yielded a trivial result in which the calculated structure factors would be identical to the starting set, including these 'inner' reflections with amplitude zero. However, transformation of the first *modified* map gave phase estimates for these hitherto unknown phases. In the

second and subsequent cycles, the amplitudes which had not been phased by MIR were combined with φ^c, the phases derived from the modified map, and a centroid figure of merit m^c calculated from the unimodal phase probability curve. Concomitantly the 2633 terms which were originally phased by MIR were handled as described in the preceding section on tethered phase improvement. After seven cycles the calculated phases for the 29 low-resolution terms had a mean error of 5° (all 22 of the centrosymmetric reflections had the correct sign and the seven non-

Fig. 5. Parameters monitoring refinement progress and phase error *vs* refinement cycle in yeast *t*RNA$_f^{\text{Met}}$ for 2662 phases from 100–4·5 Å resolution. Filled symbols designate the seven tethered cycles and open symbols the four untethered cycles. The R factor (♦) is evaluated by $\sum_h ||F_{\text{cal}}| - |F_{\text{obs}}||/\sum_h |F_{\text{obs}}|$. Also shown are cumulative phase change from the starting MIR values (■), change from the previous cycle (▲), and phase error (●).

Fig. 6. Cumulative phase change from the starting 2662 phases in the range 100–4·5 Å after seven cycles tethered refinement (□) and an additional four cycles untethered refinement (○) *vs* original MIR figure of merit.

centrosymmetric reflections had a mean error of 22°). For the entire set of structure factors extending from 100 to 4·5 Å the mean phase error was 46°. Fig. 2(*a*) shows that the additional improvement of 3° associated with phase extension to low resolution occurs over most of the resolution range, 14 to 5·0 Å. The phase change and improvement with each cycle is charted in Fig. 5.

Phasing by continued density modification not tethered to MIR

After the last cycle of tethered phase improvement and phase extension to 100 Å described above, four cycles of density modification were subsequently carried out using φ^c from the modified map, disregarding the original MIR phase probability curve. When phases were no longer tethered to the MIR phases there was an immediate movement away from the tethered centroid phases; however, the total mean phase change from the original MIR phase stabilized at 63° after four cycles of untethered refinement (Fig. 5). Although no longer tethered to the MIR phases, the new phases which showed the greatest cumulative change continued to be those with the poorest initial MIR figure of merit (Fig. 6). The large shift in the untethered phase was accompanied by an immediate additional phase improvement in the first untethered cycle of 2·5° which was increased to 3° by the fourth cycle. This further reduced the phase error to a mean value of 43°, *i.e.* an average phase improvement of 25° over the starting MIR phases (Fig. 5). The improvement which accompanies untethering covers all resolution ranges (Fig. 2*a*) and again the quality of the final phase appears nearly independent of the starting figure of merit (Fig. 2*b*).
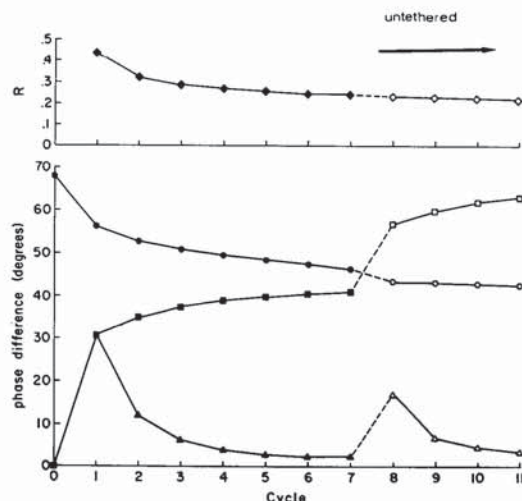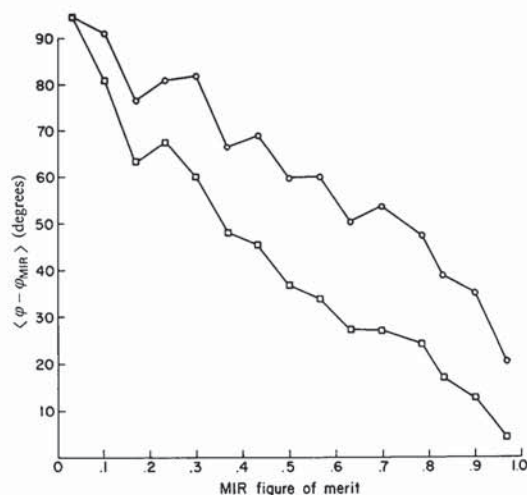
Phase extension to all terms from 100–4 Å resolution in conjunction with phase improvement

The yeast *t*RNA$_f^{\text{Met}}$ intensities had been measured to 4·0 Å, although MIR phasing was effective to only 4·5 Å (Fig. 1). Density modification was used to extend phases to higher resolution in the same manner that phases were extended to lower resolution.

The set of 2633 reflections to 4·5 Å resolution which had been phased by MIR were augmented by a total of 912 reflections not previously phased by MIR: 673 reflections recorded in the resolution zone 4·5–4·0 Å, the 29 low-resolution reflections discussed earlier, and an additional 210 reflections in the 14–4·5 Å range. With the phases of all these 912 unphased reflections arbitrarily set to zero, the mean error of the 3545 phases in the entire 100–4 Å resolution range was 74°. Seven cycles of density modification were carried out in which the phases were tethered to the original MIR phase, producing an overall phase error of 52°, an improvement of 22°. This was followed by four cycles of untethered density modification in which the phase

information produced by density modification was not merged with that of the original MIR analysis. The phases produced by density modification for the terms in the higher-resolution range of 4·5–4·0 Å which had not been phased by MIR had an average error of 65°. Thus, the phase error of these higher-resolution terms, phased solely by density modification, compared favorably with the corresponding value of 68° for the entire set of original MIR phases (Fig. 7a). Extending the phases from 4·5 to 4·0 Å neither impeded the simultaneous improvement of phases in the resolution range 14–4·5 Å nor the simultaneous phase extension to lower resolution (100–14 Å).
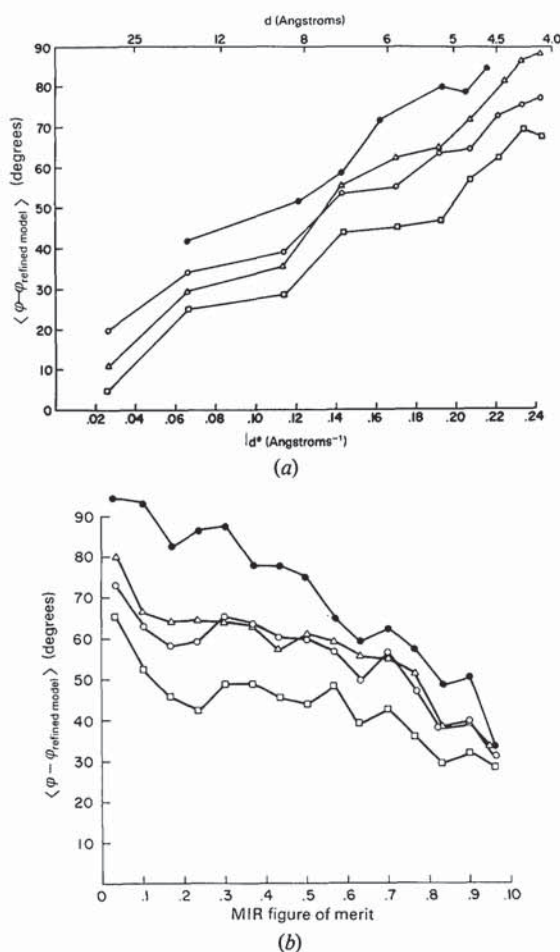

(a)

(b)

Fig. 7. Mean phase error following seven cycles tethered and four cycles untethered density modification of the 14 to 4·5 Å MIR phases with simultaneous extension to lower (100 Å) and higher (4 Å) resolution *vs* (a) resolution and (b) the figure of merit of the starting phases determined by MIR. Plotted are the mean errors for (i) the starting 2633 MIR phases (●) having 68° average phase error (74° for all 3545 reflections in the 100–4 Å zone), (ii) the 3545 phases after refinement using attenuation of negative density only (○), (iii) the 3545 phases after refinement using solvent leveling only (△), and (iv) the 3545 phases after refinement using both attenuation of negative density and solvent leveling (□).

Solvent leveling vs attenuation of negative density

To assess the individual phasing power of solvent leveling and attenuation of negative density, the phase improvement and extension procedure described above was repeated twice, once using only solvent leveling and once using only the attenuation of negative density as the method of density modification. Both components contribute to the extension of phases to the 29 'inner' (100–14 Å) reflections which had not been previously phased by MIR (Fig. 7a). Solvent leveling alone was more powerful in this low-resolution range; it produced phases with an error of 12° whereas the value obtained with just attenuating negative density was 20°. (Both together gave 5° average phase error.) As resolution increases the relative contribution from solvent leveling decreases while the contribution from attenuating negative density increases. Attenuation of negative density alone produced phases which were in error by 70° for the previously unphased terms at higher resolution (4·5–4·0 Å), whereas the corresponding effect with solvent leveling was a substantially poorer 85°.

Improvement of the electron density map

Fig. 4(a) shows the original MIR map with the phosphate backbone of the refined $tRNA_f^{Met}$ structure superimposed on the density (negative contours are not shown). Fig. 4(b) shows the cosmetic effect of just leveling the solvent and attenuating the negative density of the map shown in Fig. 4(a) and represents the appropriate point of reference for assessing the phase improvement reflected in the map shown in Fig. 4(c). Note that in the starting map (Fig. 4b) there is poorly connected density in the anticodon loop (A) and the D stem (D), and an appendage of noise at the end of the anticodon stem (N). Following phase improvement and extension a very substantial improvement in the map can be seen in Fig. 4(c). This is most easily visualized in the region of the anticodon arm where the noise, in Fig. 4(b), disappeared while the density associated with the anticodon loop and D stem backbone was strengthened.

The striking correspondence between the map produced by the final stage of density modification (Fig. 4c) and that produced by phases from the refined structure (Fig. 4d) is perhaps the strongest illustration of the method's phasing power. Of particular note is the gap (arrow) seen in the electron density of both the map calculated with phases obtained by density modification (Fig. 4c) and the map calculated with phases obtained from the refined molecular parameters. In the case of the map calculated from the refined coordinates, this gap can be attributed mainly to the fact that P(33)* has an unusually large temperature

---

* Numbering system of Sprinzl, Grüter & Gauss (1978).

factor of 250. However, the phases produced by the density modification procedures are quite independent of those calculated from the refined structure parameters and they too have produced a map with a gap at the same position. This suggests that the region around P(33) does not contribute significantly to the diffracted intensities and is indeed locally disordered.

Discussion

Leveling the solvent regions and attenuating negative density of crystalline yeast $tRNA_f^{Met}$ improved the MIR phases significantly and phased previously unphased structure factors in zones of both higher (4·5–4·0 Å) and lower (100–14 Å) resolution. The phase improvement and extension produced a striking improvement in the electron density map. Since all of the procedures were initiated with a MIR map of medium resolution (4·5 Å) and mediocre phases (68° average phase error), the method is likely to be of general value in improving the accuracy and interpretability of electron density maps of macromolecules.

Direct methods may be of particular value when applied to cases such as yeast $tRNA_f^{Met}$ where crystalline disorder ($B = 150$ Å^2) and other experimental factors limit the accuracy of the intensity measurements or otherwise compromise the application of the MIR method. Not only can these direct methods circumvent the limitations of poor derivatives but, unlike MIR techniques which depend upon accurate differences between parent and derivative amplitudes, direct methods use the full parent amplitudes with their inherently better accuracy. This is borne out by the observation that the phases determined by density modification for terms that were poorly phased by MIR approach the accuracy of those derived from terms that were well phased by MIR (Figs. 2b and 7b).

The crucial stage in any macromolecular structure determination is the interpretation of the electron density in terms of the continuous molecular backbone. Whereas recognizing specific side chains may require accurate high-resolution phases, visualizing the molecular backbone may require improvement of the electron density map at medium resolution, say 5–3 Å. Our results with yeast $tRNA_f^{Met}$ show that density modification may be particularly valuable in this context since nearly uniform phase improvement can be achieved across a wide range of resolution (Figs. 2a and 7a). This may reflect the fact that unlike real- or reciprocal-space methods based on squaring of electron density, density modification, as applied here, does not depend on assumptions of atomicity or of well defined scattering groups.

In our calculations, solvent leveling and attenuation of negative density have roughly equal and additive effects in improving phases. Thus when the molecular boundary is uncertain, asserting only the positivity of electron density (which can always be applied) will likely still yield credible phase improvement. Furthermore, we have shown that attenuating negative density alone gives very good phases for a set of 100–14 Å resolution reflections and therefore can add considerably in the crucial task of defining the molecular boundary needed for solvent leveling.

It should be pointed out that although there was no local symmetry to exploit in this study, the volume of the asymmetric unit is unusually large in comparison to the molecule. This not only facilitates the task of safely delineating a molecular envelope but presents a highly sampled molecular transform which can be considered comparable to exploiting the redundancy of locally symmetric density. Since the tRNA molecules occupy only 17·5% of the crystal's volume, i.e. about one third of the usual molecular volume fraction, the increased sampling here would be roughly comparable to a threefold molecular redundancy for the purposes of applying real-space direct methods.

Attention has already been drawn to the very close correspondence between the 'ideal map' calculated from the refined molecular parameters and that produced by phases which were improved and extended by density modification. In particular, the fact that an anomalous feature such as the gap at P(33) in the anticodon was observed in both maps lends credence to both procedures. A more detailed discussion of the anticodon loop structure as deduced from the refinement and the maps shown here will be presented elsewhere (Podjarny, Schevitz, Sussman & Sigler, 1981) but it is clear that these results serve more than simply to illustrate the phasing power of real-space direct methods; they have verified and supplemented information provided by a novel refinement (Podjarny & Sussman, 1981).

Finally, we recognize that there are many alternative procedures which might well have been applied to this crystal structure and some of these are currently under study. It is just our purpose here to show that the generally applicable procedures detailed above have achieved the objective of accurately improving and extending phases to produce a readily interpretable electron density map.

References

ABAD-ZAPATERO, C., ABDEL-MEGUID, S. F., JOHNSON, J. E., LESLIE, A. G. W., RAYMENT, I. R., ROSSMANN, M. G., SUCK, D. & TSUKIHARA, T. (1980). *Nature (London)*, **286**, 33–39.

ARGOS, P., FORD, G. C. & ROSSMANN, M. G. (1975). *Acta Cryst.* A**31**, 499–566.

BANTZ, D. & ZWICK, M. (1974). *Acta Cryst.* A**30**, 257–260.

BARRETT, A. N. & ZWICK, M. (1971). *Acta Cryst.* A**27**, 6–11.

BIESECKER, G., HARRIS, J. I., THIERRY, J. C., WALKER, J. E. & WONACOTT, A. J. (1977). *Nature (London)*, **266**, 328–333.

BLOOMER, A. C., CHAMPNESS, J. N., BRICOGNE, G., STADEN, R. & KLUG, A. (1978). *Nature (London)*, **276**, 362–368.

BLOW, D. M. & CRICK, F. H. C. (1959). *Acta Cryst.* **12**, 794–802.

BRICOGNE, G. (1976). *Acta Cryst.* A**32**, 832–847.

COLLINS, D. M., BRICE, M. D., LA COUR, T. F. M. & LEGG, M. J. (1976). In *Crystallographic Computing Techniques*, edited by F. R. AHMED, K. HUML and B. SEDLACEK, pp. 330–335. Copenhagen: Munksgaard.

COLLINS, D. M., COTTON, F. A., HAZEN, E. E. JR, MEYER, E. F. JR & MORIMOTO, C. N. (1975). *Science*, **190**, 1047–1052.

FLETTERICK, R. J. & STEITZ, T. A. (1976). *Acta Cryst.* A**32**, 125–132.

HARRISON, S. C., OLSON, A. J., SCHUTT, C. E., WINKLER, F. K. & BRICOGNE, G. (1978). *Nature (London)*, **276**, 368–373.

HENDRICKSON, W. A., KLIPPENSTEIN, G. L. & WARD, K. B. (1975). *Proc. Natl Acad. Sci. USA*, **72**, 2160–2164.

HENDRICKSON, W. A. & LATTMAN, E. E. (1970). *Acta Cryst.* B**26**, 136–143.

HOPPE, W. & GASSMANN, J. (1968). *Acta Cryst.* B**24**, 97–107.

JOHNSON, C. D., ADOLPH, K., ROSA, J. J., HALL, M. D. & SIGLER, P. B. (1970). *Nature (London)*, **226**, 1246–1247.

PODJARNY, A. D., SCHEVITZ, R. W., SUSSMAN, J. & SIGLER, P. B. (1981). In preparation.

PODJARNY, A. D. & SUSSMAN, J. (1981). In preparation.

SCHEVITZ, R. W., PODJARNY, A. D., KRISHNAMACHARI, N., HUGHES, J. J. & SIGLER, P. B. (1979). *Nature (London)*, **278**, 188–190.

SIM, G. A. (1959). *Acta Cryst.* **12**, 813–815.

SPRINZL, M., GRÜTER, F. & GAUSS, D. H. (1978). *Nucleic Acids Res.* Special Supplement r15.

SUSSMAN, J. L., HOLBROOK, S. R., CHURCH, G. M. & KIM, S.-H. (1977). *Acta Cryst.* A**33**, 800–804.

WARD, K. B., HENDRICKSON, W. A. & KLIPPENSTEIN, G. L. (1975). *Nature (London)*, **257**, 818–821.

ZWICK, M., BANTZ, D. & HUGHES, J. (1976). *Ultramicroscopy*, **1**, 275–277.

An Application of the Theory of Representations to the Estimation of the One-Phase Seminvariants of First Rank

BY M. C. BURLA AND A. NUNZI

Istituto di Mineralogia dell'Università, 06100 Perugia, Italy

C. GIACOVAZZO

Istituto di Mineralogia, Università, 70121 Bari, Italy

AND G. POLIDORI

Centro Calcolo Elettronico dell'Università, 06100 Perugia, Italy

Abstract

A procedure has been devised which uses both the estimates of the one-phase seminvariants of first rank *via* their second representations and the estimates of a special class of two-phase seminvariants *via* their first representations in order to obtain accurate estimates of the one-phase seminvariants.

1. Introduction

Probabilistic theories for the estimation of the one-phase seminvariants of first rank were supplied by various authors (*e.g.* Hauptman & Karle, 1953; Cochran & Woolfson, 1954; Naya, Nitta & Oda, 1964; Weeks & Hauptman, 1970).

The *MULTAN* procedure (Germain, Main &